ORIGINAL RESEARCH

Generation of THz frequency using PANDA ring resonator for THz imaging

MA Jalil[1]
Afroozeh Abdolkarim[2]
T Saktioto[2]
CT Ong[3]
Preecha P Yupapin[4]

[1]Ibnu Sina Institute of Fundamental Science Studies, Nanotechnology Research Alliance, Universiti Teknologi Malaysia (UTM),81310, Johor Bahru, Malaysia; [2]Institute of Advanced Photonics Science, Nanotechnology Research Alliance, Universiti Teknologi Malaysia (UTM), 81310, Johor Bahru, Malaysia; [3]Department of Mathematics, Universiti Teknologi Malaysia 81310 Skudai, Johor Bahru, Malaysia; [4]Nanoscale Science and Engineering Research Alliance (N'SERA), Advanced Research Center for Photonics, Faculty of Science, King Mongkut's Institute of Technology Ladkrabang, Bangkok 10520, Thailand

Correspondence: PP Yupapin
Nanoscale Science and Engineering Research Alliance (N'SERA), Advanced Research Center for Photonics, Faculty of Science, King Mongkut's Institute of Technology Ladkrabang, Bangkok 10520, Thailand
Tel +66 2 329 8414
Fax +66 2 329 8410
Email kypreech@kmitl.ac.th; isoqt@kmitl.ac.th

Abstract: In this study, we have generated terahertz (THz) frequency by a novel design of microring resonators for medical applications. The dense wavelength-division multiplexing can be generated and obtained by using a Gaussian pulse propagating within a modified PANDA ring resonator and an add/drop filter system. Our results show that the THz frequency region can be obtained between 40–50 THz. This area of frequency provides a reliable frequency band for THz pulsed imaging.

Keywords: THz imaging, THz technology, MRRs, PANDA, add/drop filter

Introduction

Nonlinear terahertz (THz) radiation is the electromagnetic spectrum which ranges from 30 THz to 100 GHz. It covers the region away from microwaves via mid to beyond infrared. Formerly, bulky and expensive equipment such as free electron lasers or the alternative employment of thermal sources produced weak, incoherent radiation. THz radiation gives rise to rotational and vibrating excitation of some biological molecules. THz radiation has also been used in tissue with differentiating abilities.[1] There is an increasing tendency towards THz technology for the next wave of noninvasive biomedical instruments.[2,3] THz pulse has many properties that could encourage the use of THz pulsed imaging (TPI) as a medical imaging tool. Moreover, THz waves are useful for the analysis of histopathological diagnosis, without any staining process.[4] Rayleigh scattering of electromagnetic radiation increases with the inverse of the wavelength to the fourth power. However, there is no ionization hazard for biological tissue.[5] TPI is a new technique based on broadband pulses of electromagnetic radiation of THz frequencies.[6,7] Contrast images can be obtained for different degrees of THz wave absorption for normal tissues, such as muscles, fatty tissue and cartilage, as well as cancer tissue. We can obtain THz images using a microring resonator (MRR) in a wide range of wavelengths.[8,9] The THz pulse interacts with the sample in reflection or transmission modes. The modified pulse is recorded as a time-series. The spectra information from THz pulses has been used to distinguish different types of soft tissues, such as muscle, fat, and kidney tissues.[10,11]

Methodology and results

In order to achieve a wide band frequency carrier, we propose a novel system consisting of MRRs for many communication applications such as a wireless THz communication system and faster data transfer, which requires higher carrier frequencies.[12]

773

In this paper, we use MRRs made of InGaAsP/InP material to enhance the channels of the frequency band for implementation in medical imaging.[13]

The transfer function of the system uses Gaussian beam, described by Equation 1.[14]

$$E_{i1} = A_1 \exp(i\omega_0 t) \tag{1}$$

Here A_1 is the amplitude of the optical field and t is the time for phase shift with frequency shift of ω_0. The optical outputs from the first and second ring resonators are given by Equations 2 and 3.[15,16]

$$E_{out1} = E_{i1}\left(\frac{\sqrt{1-\kappa_1)(1-\gamma_1)} - (1-\gamma_1)\exp((-\alpha L_1/2) - jK_n L_1)}{1 - \sqrt{(1-\kappa_1)(1-\gamma_1)}\exp((-\alpha L_1/2) - jK_n L_1)}\right) \tag{2}$$

$$E_{i2} = E_{out1}\left(\frac{\sqrt{1-\kappa_2)(1-\gamma_2)} - (1-\gamma_2)\exp((-\alpha L_2/2) - jK_n L_2)}{1 - \sqrt{(1-\kappa_2)(1-\gamma_2)}\exp((-\alpha L_2/2) - jK_n L_2)}\right). \tag{3}$$

Here κ is the coupling coefficient, and K represents the wave number in vacuum. γ is the fractional coupling intensity loss. L_1 and L_2 are circumferences of the first and second rings. Exp$(-\alpha L/2)$ shows the roundtrip loss coefficient and α is the waveguide loss. For the PANDA system, the output optical fields from right and left rings are expressed by Equations 4 and 5.

Therefore, the final equations for drop port and throughput power are given in Equations 10–13.

$$E_t = E_{i2}\sqrt{(1-\kappa_3)(1-\gamma_3)}$$
$$+ j\sqrt{\kappa_3(1-\gamma_3)}\sqrt{(1-\kappa_4)(1-\gamma_4)}$$
$$\times E_L E_R E_1 \exp((-\alpha L/2) - jK_n L) \tag{10}$$

$$E_d = j\sqrt{\kappa_4(1-\gamma_4)}E_1 E_R \exp((-\alpha L/4) - (jK_n L/2)) \tag{11}$$

$$P_t = (E_t)\cdot(E_t)^* = |E_t|^2 \tag{12}$$

$$P_d = (E_d)\cdot(E_d)^* = |E_d|^2. \tag{13}$$

where P_t and P_d represent the output powers of the throughput and drop port, respectively.[14,15]

In this work we use a Gaussian beam as an input power to the proposed system. The new design of the system is illustrated in Figure 1. In this case the Gaussian pulse with a center wavelength of 1.3 μm, pulse width of 20 ns, and power of 1 W, is an input into the system as shown in Figure 2A. The parameters used are R_1 = 5 μm (radius of first ring), R_2 = 3 μm (radius of second ring), R_L = 1 μm (radius of left ring of PANDA), R_R = 1 μm (radius of right ring of PANDA), R = 3 μm (radius of centered ring

$$E_R = E_1\exp((-\alpha L/8) - (jK_n L/4))\left(\frac{\sqrt{(1-\gamma_5)(1-\kappa_5)} - (1-\gamma_5)\exp((-\alpha L_R/2) - jK_n L_R)}{1 - \sqrt{(1-\gamma_5)(1-\kappa_5)}\exp((-\alpha L_R/2) - jK_n L_R)}\right) \tag{4}$$

$$E_L = E_3\exp((-\alpha L/8) - (jK_n L/4))\left(\frac{\sqrt{(1-\kappa_6)(1-\gamma_6)} - (1-\gamma_6)\exp((-\alpha L_L/2) - jK_n L_L)}{1 - \sqrt{(1-\kappa_6)(1-\gamma_6)}\exp((-\alpha L_L/2) - jK_n L_L)}\right). \tag{5}$$

Here, E_R and E_L are the outputs from the right and left rings of the PANDA system. The interior output fields of E_1, E_2, E_3, and E_4 are shown in Equations 6–9.

$$E_1 = \frac{j\sqrt{\kappa_3}\sqrt{1-\gamma_3}E_{i2}}{1 - E_R E_L\sqrt{(1-\kappa_3)(1-\kappa_4)}\exp((-\alpha L/2 - jK_n L)} \tag{6}$$

$$E_2 = E_1 E_R\exp((-\alpha L/4) - (jK_n L/2)) \tag{7}$$

$$E_3 = E_1 E_R\sqrt{(1-\kappa_4)(1-\gamma_4)}\exp((-\alpha L/4) - (jK_n L/2)) \tag{8}$$

$$E_4 = E_L E_1 E_R\sqrt{(1-\kappa_4)(1-\gamma_4)}\exp((-\alpha L/2) - jK_n L). \tag{9}$$

of PANDA), A_{eff} = 0.10–0.25 μm.[2] Some fixed parameters such as nonlinear refractive index, n_0 = 3.34 (InGaAsP/InP)[17] and intensity attenuation coefficient, α = 0.2 dBmm^{-1} have been selected for this system. The coupler intensity loss is γ = 0.1. The coupling coefficient of the MMR varies from 0.1–0.98. The nonlinear refractive index is n_2 = 2.2 × 10^{-17}.

The input pulse is sliced to a smaller signal through the spectrum shown in Figure 2B and C. The light pulse can be chopped into discrete signals and amplified in the first ring, where more signal amplification is obtained by the second ring (smaller ring). The output signals from the
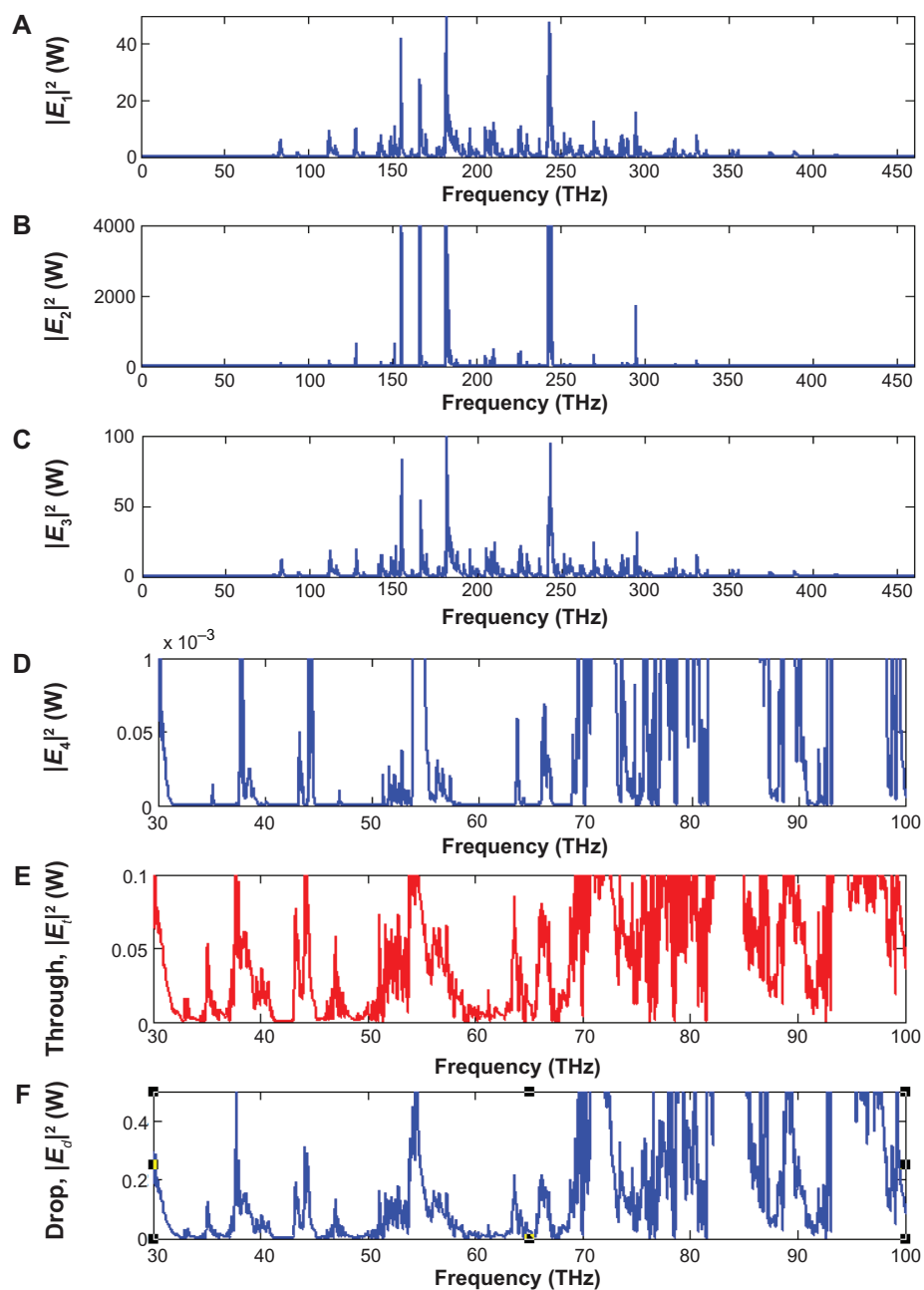
Figure 1 Schematic of two microring resonators coupled into a PANDA system.

second ring resonator are inputs into the PANDA system. Output signals of the PANDA system are simulated and shown in Figure 3A–F. Figure 3E and F show the best region of frequency, which can be seen at the range of 40–50 THz. In practice, the channel frequency can be increased by using the system. Finally, the required signals can be obtained via the PANDA system.

The output signals from the PANDA system are inputs to the add/drop filter system in order to cancel out noisy chaotic signals. To retrieve the signals from the chaotic noise, we suggest the use of add/drop filters with proper parameters.

Two complementary optical circuits of the MRR add/drop filter can be illustrated by Equations 14 and 15.[17]

$$\left|\frac{E_{t1}}{E_t}\right|^2 = \frac{(1-\kappa_1)-2\sqrt{1-\kappa_1}\cdot\sqrt{1-\kappa_2}e^{-\frac{\alpha}{2}L}\cos(k_nL)+(1-\kappa_2)e^{-\alpha L}}{1+(1-\kappa_1)(1-\kappa_2)e^{-\alpha L}-2\sqrt{1-\kappa_1}\cdot\sqrt{1-\kappa_2}e^{-\frac{\alpha}{2}L}\cos(k_nL)}$$

(14)

$$\left|\frac{E_{t2}}{E_t}\right|^2 = \frac{\kappa_1\kappa_2 e^{-\frac{\alpha}{2}L}}{1+(1-\kappa_1)(1-\kappa_2)e^{-\alpha L}-2\sqrt{1-\kappa_1}\cdot\sqrt{1-\kappa_2}e^{-\frac{\alpha}{2}L}\cos(k_nL)},$$

(15)

Figure 2 Result of the outputs from two ring resonators with centre wavelength at 1.3 μm: (**A**) the input Gaussian pulse, (**B**) the chaotic signal generation, (**C**) the amplified and filtering signals.

Figure 3 Simulation results of the light pulse generated by the PANDA system at center wavelength of 1.3 μm, where (**A**) $|E_1|^2$, (**B**) $|E_2|^2$, (**C**) $|E_3|^2$, (**D**) $|E_4|^2$, (**E**) $|E_t|^2$, and (**F**) $|E_t|^2$ are output powers inside a PANDA system.

where E_{t1} and E_{t2} represent the optical fields of the throughput and drop port, respectively. $\beta = kn_{eff}$ is the propagation constant, n_{eff} is the effective refractive index of the waveguide, $L = 2\pi R$ is the circumference of the ring, and R is the radius of the ring. For simplification, we define the phase constant as $\phi = \beta L$. Chaotic noise cancellation and required signals can be obtained by using the particular parameters of the add/drop device. κ_1 and κ_2 are coupling coefficients of the add/drop filters, $\kappa_n = 2\pi/\lambda$ is the wave propagation number for a vacuum, where the waveguide
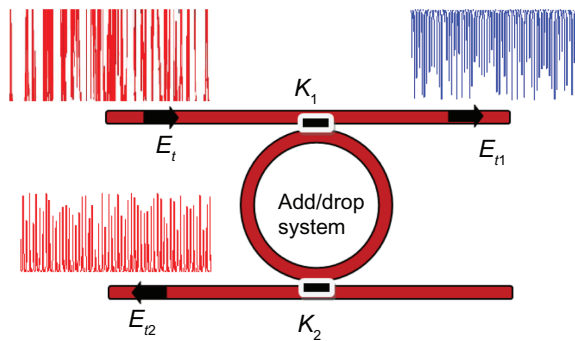
Figure 4 Schematic of an add/drop filter system for area frequency selection.
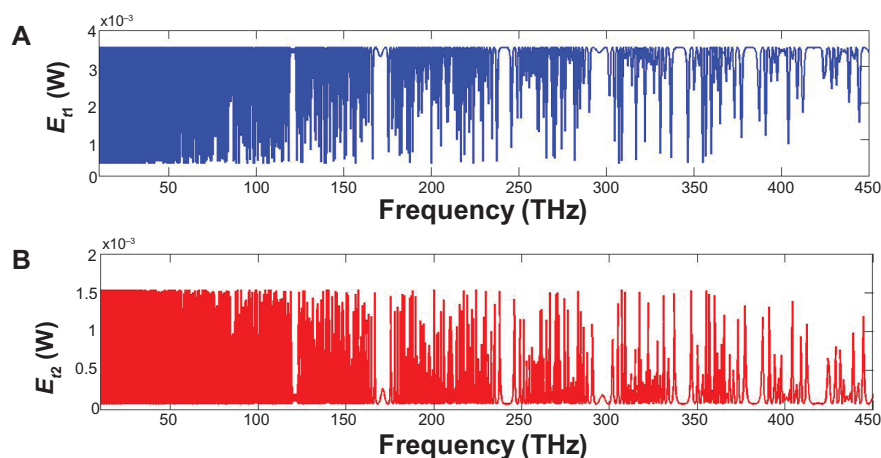
Figure 5 Simulation results of the channel frequency light pulse generated by the add/drop filter system at the center wavelength of 1.3 μm for Gaussian pulse: (**A**) system throughput, (**B**) system drop port.

loss is $\alpha = 0.2 \ dB$/mm. The fractional coupler intensity loss is $\gamma = 0.1$. For the add/drop filter device, the nonlinear refractive index is neglected.

We used an add/drop filter system with a radius of 10 μm to determine the free spectral range, the number of channels and bandwidth as shown in Figure 4. Figure 5 shows the simulation results where Figure 5A and B represent the throughput and drop port outputs of the system, respectively.

As demonstrated in Figure 6, generated dense wavelength-division multiplexing from the proposed configuration of ring resonators are involved in the THz region, which provides a reliable frequency band for medical applications, especially for THz imaging. The main advantage of THz imaging is

its diagnostic capabilities.[11] These obtained pulses are also useful for analysis of the histopathological diagnosis, without any staining process.[6]

To date, imaging spectroscopy is used only for small areas.[3,4] THz imaging exactly reflects the tissue situation, for instance tumor, nontumor tissues, tissue degeneration, and fibrosis. The THz image shows significantly reduced absorption of THz radiation in this region compared with normal tissue, which suggests its usefulness for detecting tumors (Figure 7). Contrast images associated with different degrees of absorption of THz waves have been obtained for normal tissues, such as muscles, fatty tissue, and cartilage, as well as for cancer tissue. We could obtain THz images of large areas from an MRR in a wide range of wavelengths.[8,10,11]
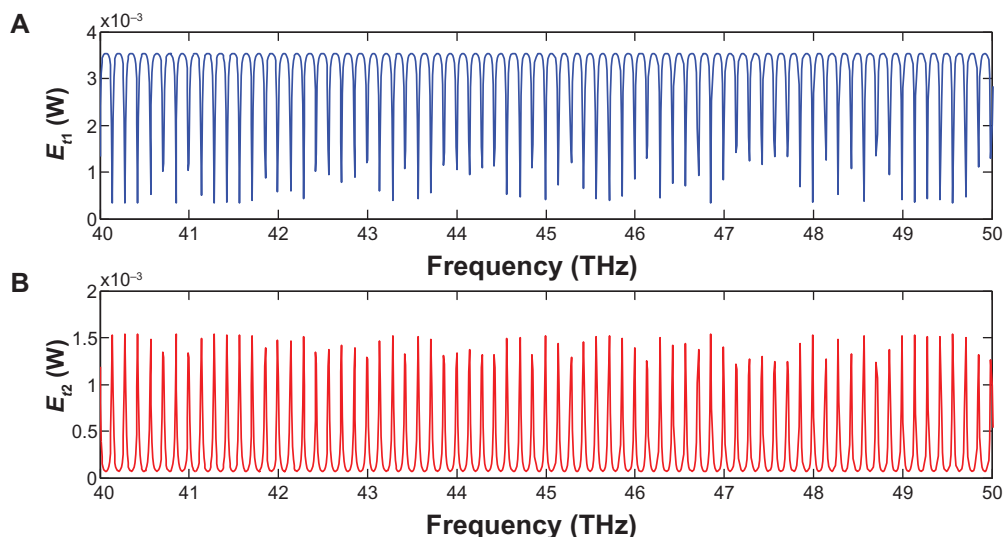

Figure 6 Expansion of simulation result of the channel frequency light pulse generated by the add/drop filter system.
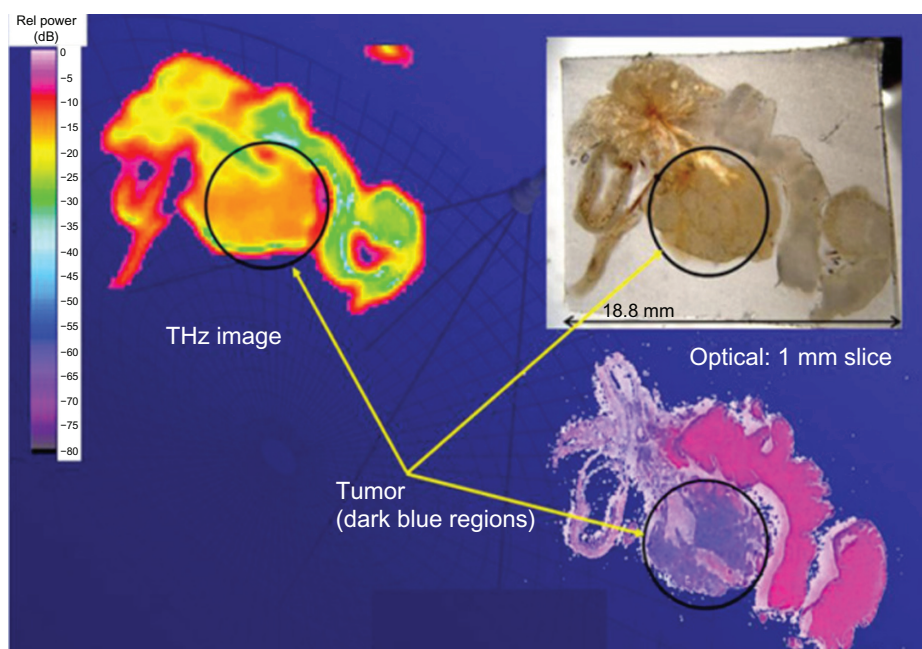
Figure 7 Prostate section with tumor tissue as imaged with terahertz, optical, and staining techniques.

Conclusion

In this study, a new MRR design has been introduced, which provides the best frequency band when the input Gaussian pulse is used. This system consists of a series of MRRs connected to a PANDA system. Using the proposed system, multifrequency bands can be generated and simultaneously linked to an add/drop filter where it is suitable for analysis of the histopathological diagnosis. The results show the frequency band region lies between 40–50 THz. This range provides a reliable frequency band for medical purposes, especially in THz imaging.

Acknowledgments

References

1. Mittleman MD, Jacobson RH, Nuss MC. T-ray imaging. *IEEE J Sel Top Quant Electron*. 1996;2:679–692.
2. Iglesias EJ, Smith AW, Kaplan SG. A sensitive, spatially uniform photo-detector for broadband infrared spectrophotometry. *Appl Opt*. 2008;47: 2430–2436.
3. Arnone D, Ciesla C, Pepper M. Terahertz imaging comes into view. *Phys World*. 2000;13:35–40.
4. Knobloch P, Schildknecht C, Kleine-Ostmann T, et al. Medical THz imaging: An investigation of histo-pathological samples. *Phys Med Biol*. 2002;47:3875–3884.
5. Fitzgerald A, Berry E, Zinovev N, Walker GC, Smith MA, Chamberlain JM. An introduction to medical imaging with coherent terahertz frequency radiation. *Phys Med Biol*. 2002;47: R67–R84.
6. Hu B, Nuss M. Imaging with terahertz waves. *Opt Lett*. 1995;20: 1716–1718.
7. Zhang X. Generation and detection of pulsed microwave signals by THz optoelectronics. Proceedings of 1997 SBMO/IEEE MTT-S International Microwave and Optoelectronics Conference, 1997. Linking to the Next Century. Natal, Brazil. August 11–14, 1997;1: 215–220.
8. Nishizawa JI, Sasaki T, Suto K, et al. THz imaging of nucleobases and cancerous tissue using a GaP THz-wave generator. *Opt Comm*. 2005; 244(1–6):469–474.
9. Wallace VP, Taday PF, Fitzgerald AJ, et al. Terahertz pulsed imaging and spectroscopy for biomedical and pharmaceutical applications. *Faraday Discuss*. 2004;126:255–263.
10. Fitzgerald AJ, Wallace VP, Jimenez-Linan ML, et al. Terahertz pulsed imaging of human breast tumors. *Radiology*. 2006;239: 533–540.
11. Nakajima S, Hoshina H, Yamashita M, Otani C, Miyoshi N. Terahertz imaging diagnostics of cancer tissues with a chemometrics technique. *Appl Phys Lett*. 2007;90:041102.
12. Udomariyasap P, Noppanakeepong S, Mitatha S, Yupapin PP. THz light pulse generation and storage within an embedded optical waveguide system. *J Nonlinear Opt Phys*. 2010;19:303–310.
13. Grover R, Absil PP, Van V, et al. Vertically coupled GaInAsP-InP micror-ing resonators. *Opt Lett*. 2001;26:506–508.
14. Juleang P, Phongsanam P, Mitatha S, Yupapin PP. Public key suppres-sion and recovery using a PANDA ring resonator for high security communication. *Opt Eng*. 2011;50:035002.

15. Yupapin PP, Vanishkorn B. Mathematical simulation of light pulse propagating within a microring resonator system and applications. *Appl Math Model*. 2011;35:1729–1738.

16. Amiri IS, Afroozeh A, Bahadoran M. Simulation and analysis of multisoliton generation using a PANDA ring resonator system. *Chinese Phys Lett*. 2011;28:104205.

17. Piyatamrong B, Kulsirirat K, Techitdheera W, Mitatha S, Yupapin PP. Dynamic potential well generation and control using double resonators incorporating an add/drop filter. *Mod Phys Lett B*. 2010;24:3071–3080.